



## Article

# Assessing the Performance of Multipath Mitigation for Multi-GNSS Precise Point Positioning Ambiguity Resolution

Kai Zheng <sup>1,2,3</sup> , Lingmin Tan <sup>1</sup> , Kezhong Liu <sup>1,2,3,\*</sup> , Mozi Chen <sup>1,2,3</sup> and Xuming Zeng <sup>1,2,3</sup>

<sup>1</sup> School of Navigation, Wuhan University of Technology, Wuhan 430063, China; kzheng@whut.edu.cn (K.Z.); lim.t@whut.edu.cn (L.T.); chenmz@whut.edu.cn (M.C.); zengxvming@whut.edu.cn (X.Z.)

<sup>2</sup> National Engineering Research Center for Water Transport Safety, Wuhan University of Technology, Wuhan 430063, China

<sup>3</sup> Hubei Key Laboratory of Inland Shipping Technology, Wuhan 430063, China

\* Correspondence: kzliu@whut.edu.cn

**Abstract:** Real-time GNSS PPP is commonly used for high-precision positioning, but its utility is constrained by factors that necessitate extended convergence periods for a dependable accuracy. Multipath, as an unmodeled error, significantly curtails PPP performance in time-constrained scenarios. Approximately 31 consecutive days of multi-GNSS data from the satellite positioning service of the German national survey (SAPOS) network were collected to evaluate the effectiveness of multipath correction for real-time PPP ambiguity resolution (AR). Using principal component analysis (PCA) to extract the common-mode error (CME) from observation residuals prior to multipath modeling, a multipath hemispherical map (MHM) and sidereal filtering (SF) approach were employed to alleviate the effects of multipath and assess the efficacy of multipath correction in real-time PPP-AR. The average RMS reductions of the carrier-phase and pseudorange residual of multi-GNSS were 25.5% and 20.1% with MHM<sub>0.5</sub>, while being 24.4% and 18.3% using SF. With MHM<sub>0.5</sub> correction, the TTFF reductions were approximately 7.0%, 17.7%, 37.5%, and 23.7% for G/GE/GC/GEC kinematic PPP-AR, respectively; and the convergence times for G/GE/GC PPP-AR were reduced to 18.2, 11.7, and 8.6 min, while GEC achieved an average convergence time of 7.1 min; a remarkable improvement compared to the multipath-uncorrected result (18 min). Moreover, 80% of the stations achieved convergence within 10 min, while 40% achieved convergence within 5 min. The kinematic positioning accuracy for the GEC solution improved from 0.97, 0.88, and 2.07 cm, to 0.94, 0.70, and 1.72 cm. In the static results, the TTFF shortened by 30.1%, 19.1%, and 20.1% for G/GE/GC, and the GEC decreased from 10.5 to 9.7 min; the average convergence time for G/GE/GC shortened to 13.0, 10.0, and 11.3 min, and for GEC shortened from 12.5 to 8.3 min. For the GPS-only solution, 78.3% of stations achieved convergence within 15 min. Similarly, for the GE scheme, the convergence time was primarily concentrated within 10 min, and for GC and GEC, with the application of enhanced multipath error correction, some of the stations even achieved convergence of PPP-AR within 5 min. The static positioning accuracy for GEC PPP was 0.50, 0.30, and 0.71 cm for the east, north, and up components.

**Keywords:** multi-GNSS; multipath; precise point positioning; ambiguity resolution; time to first fix; convergence time



**Citation:** Zheng, K.; Tan, L.; Liu, K.; Chen, M.; Zeng, X. Assessing the Performance of Multipath Mitigation for Multi-GNSS Precise Point Positioning Ambiguity Resolution. *Remote Sens.* **2023**, *15*, 4137. <https://doi.org/10.3390/rs15174137>

Academic Editor: Michael E. Gorbunov

Received: 18 July 2023

Revised: 13 August 2023

Accepted: 20 August 2023

Published: 23 August 2023



**Copyright:** © 2023 by the authors. Licensee MDPI, Basel, Switzerland. This article is an open access article distributed under the terms and conditions of the Creative Commons Attribution (CC BY) license (<https://creativecommons.org/licenses/by/4.0/>).

## 1. Introduction

Global navigation satellite system (GNSS) precise point positioning (PPP) is a reliable and resilient technique that is extensively employed in applications requiring high-precision positioning [1]. However, the long convergence time of at least 30 min needed for GPS to achieve centimeter-level positioning accuracy severely affects the efficiency of crustal deformation monitoring [2], seismic waveform acquisition [3], and real-time water vapor monitoring [4]. To advance the use of PPP in applications that require quick positioning, it is crucial to reduce the convergence time and improve accuracy.

Numerous studies have been devoted to ambiguity resolution (AR) [5,6]. Compared to the PPP float solution, GPS PPP-AR can significantly decrease the convergence time to approximately 20 min and improve the positioning accuracy by 54% [7]. At present, BDS has been fully deployed and offers global positioning services. As for the Galileo system, 26 satellites are in orbit [8]. Benefiting from observation redundancy and improved satellite geometry, PPP positioning accuracy and reliability are expected to improve. With GPS and BDS combined, the time to first fixed (TTFF) ambiguity was shortened to 16.9 and 24.6 min for static and kinematic modes, respectively [9]. Li et al. [10] assessed the performance of GPS+ Galileo+ BDS (GEC) PPP-AR and demonstrated that an average three-dimensional (3D) positioning accuracy could be achieved of 2.2 cm and the average convergence time was within 10.8 min. In addition to the coupling between parameters, unmodeled errors, such as multipath errors, are the primary factors hindering the performance of PPP [11].

A favorable environment with less specular reflection from the surrounding obstacles can reduce the multipath effect to some extent, but the selection of station locations is constrained by various factors in practical applications. Hardware-based techniques cannot entirely mitigate the multipath effect and are costly [12]. In recent years, research on multipath elimination has mainly been based on software data processing, such as employing signal-to-noise ratio (SNR) [13] and wave-based approaches to extract multipath [14]. Apart from multipath reduction techniques based on stochastic models, and the decomposition and filtering of observed signals, researchers have also explored modeling modifications based on the spatio-temporal repetitive characteristics of multipath. Assuming the surrounding environment of the station remains constant, the multipath is only considered to be related to the geometric position of the satellite and the station, corresponding to the repetition of satellite geometry. Genrich and Bock [15] employed the sidereal filtering (SF) approach to mitigate multipaths by exploiting the orbital repeat time (ORT), which is almost a sidereal day for GPS satellites. However, the ORT differed slightly for each satellite. Choi et al. [16] showed that the ORT of GPS satellites was approximately 9 s earlier than the generally assumed 23 h 56 m 4 s. Subsequently, Ragheb et al. [17] comprehensively considered the satellite geometry-repeat lag and calculated the ORT for individual satellites. The ORT carries the risk of being affected by orbital maneuvers, thereby deteriorating SF performance [18]. In general, multipath extraction and mitigation studies are primarily based on relative positioning techniques [19]. However, these methods are reliant on the reference station being free from multipaths, and it is difficult to separate and extract the multipath for each station. Hence, numerous researchers have attempted to extract multipaths using the PPP technique. Atkins et al. [20] verified that multipath alleviation in the observation domain is more effective than in the coordinate domain for PPP, as the corrected observation can produce a more stable position result.

The correction method for spatial domain repeatability based on multipath has been extensively researched and can be effectively utilized in real-time applications. Cohen constructed a spherical harmonic model of 12 harmonics based on a spherical harmonic function, which is equivalent to dividing a  $360^\circ \times 90^\circ$  sky map into a  $30^\circ \times 30^\circ$  grid in modeling [21]. However, it is difficult to combine accuracy and efficiency, due to the high computational complexity of high-order spherical covariance models. Fuhrmann et al. [22] proposed multipath stacking (MPS), which can realize high-resolution modeling by using the equal area method to partition the sky grid; this method has a better effect on low-frequency multipaths but ignores the spatial distribution of multipaths in the grid and has limited effects on high-frequency multipath correction. Dong et al. [23] identified the look-up table methods, collectively referred to as the multipath hemisphere mapping (MHM) model, which corrects the multipath directly based on the theory that the multipath is related to the azimuth and elevation of the satellite. On this basis, numerous researchers have attempted to fit the spatial distribution of a multipath within a grid or refine the grid size to capture high-frequency multipaths, thereby improving the robustness of the multipath model [24–26]. Zhang et al. [27] systematically evaluated the performance of MHM models, which were separately modeled for different systems, frequencies, and satel-

lite types in BDS2/BDS3. Additionally, this research contributes to relative positioning. Lu et al. [28] employed trend surface analysis-based MHM for PPP, resulting in notable enhancements in positioning accuracy and convergence time. Meanwhile, Zheng et al. [29] investigated the effectiveness of multipath mitigation on UPD estimation and PPP-AR, but only using GPS observation.

Considering these factors, this study assesses the efficacy of multipath correction for real-time PPP-AR, implementing a principal component analysis (PCA), in order to combat the effects of common-mode errors (CME), and comparing and analyzing the correction effects of two classic algorithms, MHM and SF. Furthermore, a comparative analysis was conducted on different combinations of systems, PPP-AR. In this study, the principle of the multipath extraction and modeling approach is introduced in Section 2, followed by a detailed description of the dataset and strategy in Section 3. Section 4 evaluates TTFF, convergence time, and positioning accuracy as primary PPP-AR indicators. Finally, the conclusions are presented in Section 5.

## 2. Methods

### 2.1. Multipath Extraction

The observation equations for the single-site GNSS dual-frequency raw pseudorange  $P_{r,j}^s$  and carrier-phase measurements  $L_{r,j}^s$  can be expressed as follows:

$$\begin{cases} P_{r,j}^s = \rho_r^s + \mu_j \gamma_{r,1}^s + c(t_r - t^s) + d_{r,j} - d_j^s + T_r^s + M_{r,j}^s + \zeta_{r,j}^s \\ L_{r,j}^s = \rho_r^s - \mu_j \gamma_{r,1}^s + c(t_r - t^s) + b_{r,j} - b_j^s + T_r^s + \lambda_j N_{r,j}^s + m_{r,j}^s + \varepsilon_{r,j}^s \end{cases} \quad (1)$$

where  $\rho_r^s$  represents the geometric distance from the receiver  $r$  to satellite  $s$ , which has absorbed the troposphere delay;  $\gamma_{r,1}^s$  denotes the ionospheric delay on the first frequency and  $\mu_j = \lambda_j / \lambda_1$  defined as the scale factor relative to the first frequency;  $t_r$  and  $t^s$  represent the receiver clock offset and satellite clock;  $N_{r,j}^s$  denotes the float ambiguity, while  $\lambda_j$  corresponds to the wavelength;  $d_{r,j}$  and  $d_j^s$  are the frequency-dependent hardware biases of the pseudorange for the station and satellite, respectively. Similarly,  $b_{r,j}$  and  $b_j^s$  represent the frequency-dependent phase hardware bias.  $T_r^s$  is the slant tropospheric delay;  $M_r^s$  and  $m_r^s$  refer to the multipaths of pseudorange and carrier-phase observations;  $\zeta_r^s$  and  $\varepsilon_r^s$  are the measurement noise.

The ionosphere-free (IF) combination model is typically used to eliminate the adverse effects of first-order ionospheric delays through a linear combination, while other high-order ionospheric delays are generally negligible. The multi-GNSS observation equations can be written as follows [30,31]:

$$\begin{cases} P_{r,IF}^s = \rho_r^s + c(t_r - t^s) + T_r^s + d_{r,IF} - d_{IF}^s + M_{r,IF}^s + \zeta_{r,IF}^s \\ L_{r,IF}^s = \rho_r^s + c(t_r - t^s) + T_r^s + \lambda_{IF} \cdot (N_{r,IF}^s + b_{r,IF} - b_{IF}^s) + m_{r,IF}^s + \varepsilon_{r,IF}^s \end{cases} \quad (2)$$

where

$$\begin{cases} d_{r,IF} = (f_1^2 b_{r,1} - f_2^2 b_{r,2}) / (f_1^2 - f_2^2) \\ d_{IF}^s = (f_1^2 b_1^s - f_2^2 b_2^s) / (f_1^2 - f_2^2) \\ N_{r,IF}^s = c(f_1 N_{r,1}^s - f_2 N_{r,2}^s) / (f_1^2 - f_2^2) / \lambda_{IF} \end{cases} \quad (3)$$

In float ambiguity solution PPP processing, the phase delay is linearly related to and absorbed by the ambiguity parameter. Furthermore, the estimated receiver clock error absorbs the ionosphere-free combined pseudorange hardware delay at the receiver, as the pseudorange observations provide an absolute reference for the receiver clock error. After correcting the satellite orbit and clocks, we obtain

$$\begin{cases} p_{r,IF}^s = -\mathbf{e}_r^s \mathbf{r}_r + c\bar{t}_r + T_r^s + \bar{M}_{r,IF}^s + \bar{\zeta}_{r,IF}^s \\ l_{r,IF}^s = -\mathbf{e}_r^s \mathbf{r}_r + c\bar{t}_r + T_r^s + \lambda_{IF} \bar{N}_{IF}^s + \bar{m}_{r,IF}^s + \bar{\varepsilon}_{r,IF}^s \\ \bar{N}_{r,IF}^s = N_{r,IF}^s + (b_{r,IF} - d_{r,IF}) / \lambda_{IF} - (b_{IF}^s - d_{IF}^s) / \lambda_{IF} \\ c\bar{t}_r = ct_r + d_{r,IF} \end{cases} \quad (4)$$

where  $p_{r,IF}^s$  and  $l_{r,IF}^s$  represent the observed minus computed (OMC) values for the pseudorange and carrier-phase observations, referring to the residual that remains after subtracting the estimated pseudorange or phase from the actual measurement.  $e_r^s$  is the unit vector of the direction;  $r_r$  represents the vector of the receiver position increments relative to the a priori position, and  $ct_{r,IF}^s$  represents the receiver clock correction term, which absorbs  $d_{r,IF}$ . The coordinate parameters are fixed to an a priori value, which is specified by the SAPOS Stationsparameter file, and the receiver clock offset is assumed to be white noise. In addition, there are current and mature models for phase wind-up, tidal load, phase center offset, and variation (PCO and PCV) correction [32]. Pseudorange multipath and noise represent the foremost unmodeled errors in PPP [33]. According to earlier studies, investigating carrier-phase multipath is also a worthwhile endeavor in PPP [34]. Assuming corrections for other error sources have been made, multipath and noise are the main remaining contributors to PPP residuals and the possibility of CME.

$$\begin{cases} \bar{M}_r^s = p_{r,IF}^s - ct_{r,IF}^s - T_r^s - \zeta_r^s \\ \bar{m}_r^s = l_{r,IF}^s - ct_{r,IF}^s - T_r^s - \lambda_{IF} \bar{N}_{IF}^s - \varepsilon_r^s \end{cases} \quad (5)$$

## 2.2. Multipath Modeling

This study utilized the MHM and SF approach to mitigate multipath errors. In both methods, we individually model multipaths for different systems. Specifically, for BDS, we independently modeled inclined geosynchronous orbit (IGSO) and medium earth orbit (MEO) satellite multipaths separately. The MHM grid was divided into specific resolution cells, and the PPP residuals were assigned to these cells based on the azimuth and elevation angles [29], then the effect of multipath correction for real-time PPP-AR was explored. The precise satellite orbital period is necessary for the SF method. The precise satellite orbital period  $T$  is necessary for the SF method, which is calculated using [35]:

$$n = \sqrt{GM/a^3} + \Delta n \quad (6)$$

$$T = \frac{2\pi}{n} \quad (7)$$

where  $n$  and  $\Delta n$  are the angular velocity of the satellite and the correction parameter of the angular velocity, respectively;  $\sqrt{GM}$  denotes the universal gravitational constant of the Earth ( $1.996498 \times 10^7$ ) and denotes the semi-major axis of the orbit ellipse. Considering the influence of the orbit inclination and Earth's rotation period, the ORTs for multi-GNSS satellites are separately calculated using

$$\begin{cases} ORT_G = 2T_G \\ ORT_E = 17T_E \\ ORT_{C\_MEO} = 13T_{C\_MEO} \\ ORT_{C\_IGSO} = 2T_{C\_IGSO} \end{cases} \quad (8)$$

where  $ORT_S$  and  $T_S$  are the orbital repeat time and precise satellite orbital period for satellites, respectively. The superscripts G, E, and C in the formulas represent the GPS, Galileo, and BDS systems. Generally, the ORT for GPS satellites is 86,155 s, approximately a sidereal day; for BDS, the IGSO ORT is approximately one sidereal day, while that of MEO satellites is 603,097 s, which is approximately seven sidereal days. The Galileo satellites have the longest ORT, which is approximately 10 sidereal days. The residuals of the PPP-AR model are obtained for consecutive days using both carrier-phase and pseudorange measurements.

## 3. Experiments and Results

### 3.1. Data Description and Experimental Strategy

We selected 23 multi-GNSS stations from the satellite positioning service of the German satellite positioning service (SAPOS), as shown in Figure 1. The GPS, Galileo, and BDS

observations with a 15 s sampling rate from DOY 237 to DOY 267 in 2021 were used in this study <https://www.opengeodata.nrw.de/> (accessed on 1 January 2023). Precise clock and orbit products were provided by the German Research Centre for Geosciences (GFZ). BDS geostationary orbit (GEO) satellites were excluded, as they have inadequate orbital and clock accuracies [36]. The typical ambiguity resolution method proposed by Ge et al. [37] was used for PPP-AR, which estimated the ambiguity as a constant value for each epoch. The study conducted by Lu et al. [28] indicated that the optimal modeling for GPS was 4–7 days. The BDS and Galileo satellites require a longer ORT, while multipath is subject to the site environment and will reduce the similarity over time. In this study, 5 repeat cycles were used for GPS multipath modeling, and 3 repeat cycles of data were used for BDS and Galileo modeling.

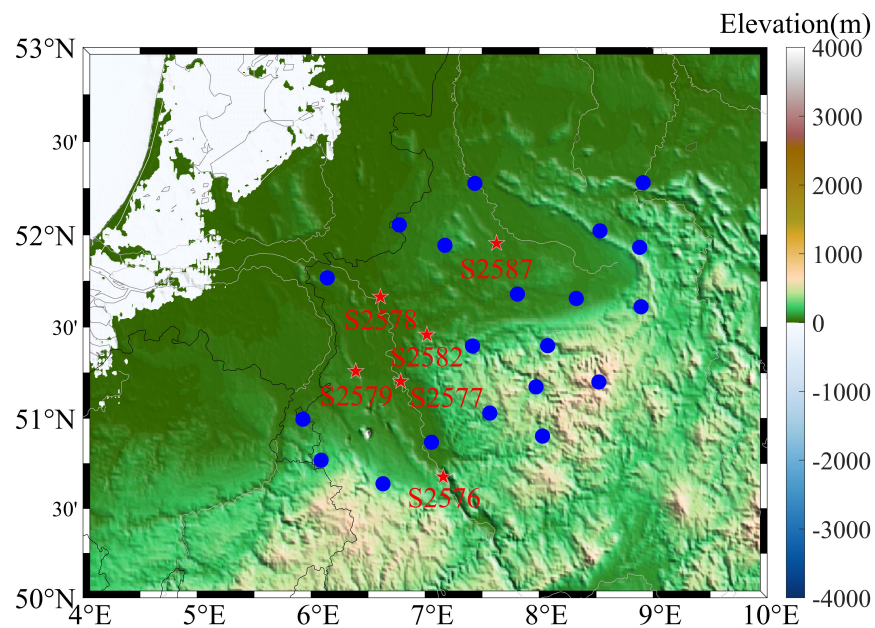


**Figure 1.** Geographical distribution of 23 SAPOS stations.

Table 1 shows the details of the data processing and error correction. To ensure accuracy, a quality control procedure was implemented to eliminate any outliers present in the residuals [22]. The common mode error (CME) was then mitigated using principal component analysis [38]. Subsequently, the residuals were allocated to a grid based on the azimuth and elevation angles. Finally, a stacking method was employed to calculate multipath correction, as outlined in the MHM model.

The ORT requirement for BDS and Galileo satellites is longer compared to that of GPS. Additionally, the impact of multipath on the similarity of data reduces over time, due to site-specific environmental factors. The GPS multipath modeling utilized a dataset spanning five days, while the BDS and Galileo modeling employed a dataset spanning 30 days. The details of the experimental scheme are provided in Table 2. We compared the results obtained without multipath correction (Uncor) as a reference with the results obtained after applying multipath correction (Cor).

**Table 1.** Data processing strategies.

Items	Strategies
Observations	GPS(L1/L2) Galileo(E1/E5a) BDS(B1/B3)
Measuremen noise	Pseudorange/phase: 0.3 m/3 mm
Estimator	Least-squares estimator for generating phase residuals
PPP-AR Strategy	Partial ambiguity resolution [39]
Samling rate	15 s
Elevation cut off	10°
Satellite orbit/clock	GFZ precise products
PCO/PCV	igs_14.atx
Tropodpheric	Dry delay corrected by the model [40] +Wet delay estimated by random walk
Ionospheric	Ionosphere-free combination
DCB	Corrected using CODE final DCB products
ISB	White noise(GPS as reference)
Receiver clock	Estimated as white noise
Station coordinate	Estimated as white noise (Kinematic)/Estimated at each epoch as constant (Static)

**Table 2.** Processing schemes designed for PPP-AR multipath correction.

Solution	Scheme	Kinematic (K) /Static (S)	Corrected (Cor) /Uncorrected (Uncor)
G	MHM <sub>0.5/1/2</sub> /SF	K/S	Cor/Uncor
GE	MHM <sub>0.5</sub> /SF	K/S	Cor/Uncor
GC	MHM <sub>0.5</sub> /SF	K/S	Cor/Uncor
GEC	MHM <sub>0.5</sub> /SF	K/S	Cor/Uncor

### 3.2. Effectiveness of Multipath Mitigation

The root mean square (RMS) reduction value for all observed satellite residuals was calculated, to indicate the effectiveness of the different methods for multipath correction using the following equation:

$$RMS_{uncor} = \sqrt{\frac{\sum_{i=1}^N X_i^2}{N}} \quad (9)$$

where  $X_i$  represents the raw pseudorange or carrier-phase residuals, and  $N$  denotes the number of epochs. The residual reduction percentage was calculated as follows:

$$V_{rms} = (RMS_{uncor} - RMS_{cor}) / RMS_{uncor} \times 100\% \quad (10)$$

where  $RMS_{uncor}$  and  $RMS_{cor}$  denote the RMS of the residuals before and after the multipath correction, respectively. We calculated the multipath corrections from the residuals according to the multipath characteristics, so other unmodeled errors were not corrected, therefore the RMS reduction result could be considered the contribution of multipath correction.

The effectiveness of the different resolution MHM models for GPS PP-AR multipath correction was assessed as shown in Figure 2. The site number was used to categorize the number of 23 stations, such as station 2576, 2577, and 2578. For an MHM resolution of 0.5/1/2, the average RMS reductions of the carrier-phase residual were 22.4%, 18.7%, and 13.8%, respectively. The pseudorange values were 20.18%, 14.2%, and 8.8%, respectively. Theoretically, as the grid resolution increases, the grid size decreases, and a relatively small grid size reduced the robustness of the MHM model. In our experiments, the performance

of the MHM deteriorated with the increase in grid size, and the optimal resolution was  $0.5^\circ \times 0.5^\circ$ , which will be addressed in the following discussion.

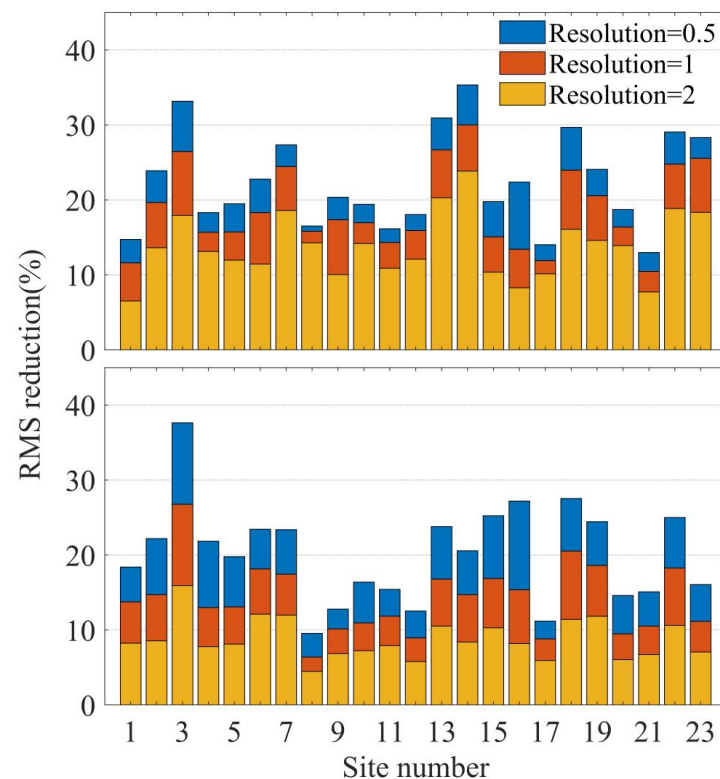


**Figure 2.** Averaged RMS reduction in the carrier-phase (top) and pseudorange (bottom) residuals for GPS-only PPP-AR.

Figure 3 shows the phase RMS reduction after the multipath correction using an  $MHM_{0.5}$  ( $MHM$  model with a  $0.5^\circ \times 0.5^\circ$  resolution) observable satellite at each station. Among them, 1–32 were GPS, 33–68 were Galileo, and 69–105 were BDS satellites. Compared with Figure 4, the reduction percentage of pseudorange residual RMS was generally lower than that of the carrier-phase, which was primarily attributed to the large error of pseudorange observation, as well as the presence of numerous gross errors that diminished the correlation between the model and real-time multipath. Table 3 presents the average percentages of RMS reduction achieved by the  $MHM_{0.5}$  and SF models applied to real-time PPP-AR multipath correction. When calculating the mean percentage reduction in multipath corrected RMS, all satellites at all stations were considered indiscriminately, the average RMS reductions of the carrier-phase and pseudorange residuals of multi-GNSS were 25.5% and 20.1% with  $MHM_{0.5}$ . In comparison, the SF model yielded reductions of 24.4% and 18.3% for carrier-phase and pseudorange residuals, respectively. As summarized in Table 3, the  $MHM_{0.5}$  and SF models exhibited comparable performance, with  $MHM_{0.5}$  showing a slight superiority over SF. One probable reason for this phenomenon was that SF can introduce additional noise when applied to real-time processing. Furthermore, the effectiveness of multipath corrections for GPS satellites is better than for the Galileo and BDS satellites. The environment around the station experienced relatively less interference in the short term, and the ORT of GPS satellites was shorter than that for Galileo and BDS. Thereby, permitting the GPS satellites to obtain a more pronounced multipath correction model for real-time applications. In addition, the partial residuals of the satellites on modeling days had little similarity, thereby reducing the multipath correction efficiency.

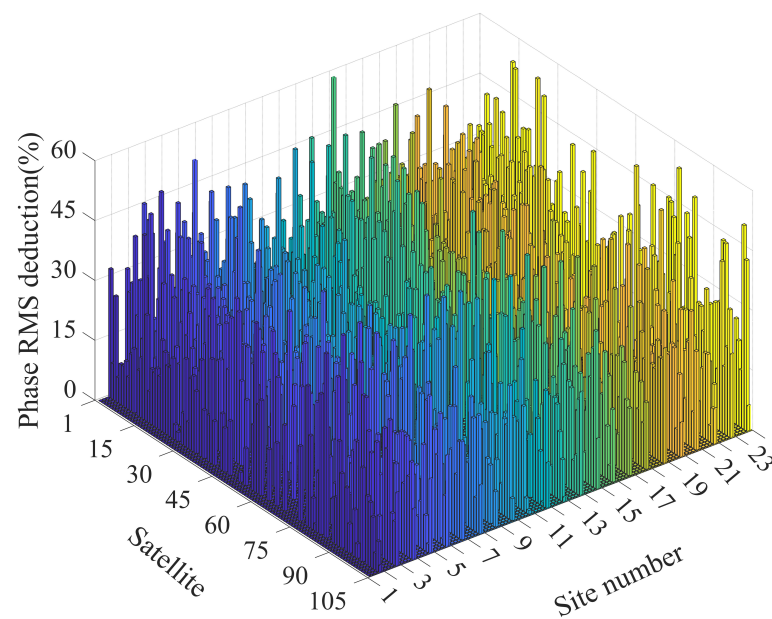


**Figure 3.** RMS reduction for carrier-phase observation by  $MHM_{0.5}$  on DOY 267 in 2021.

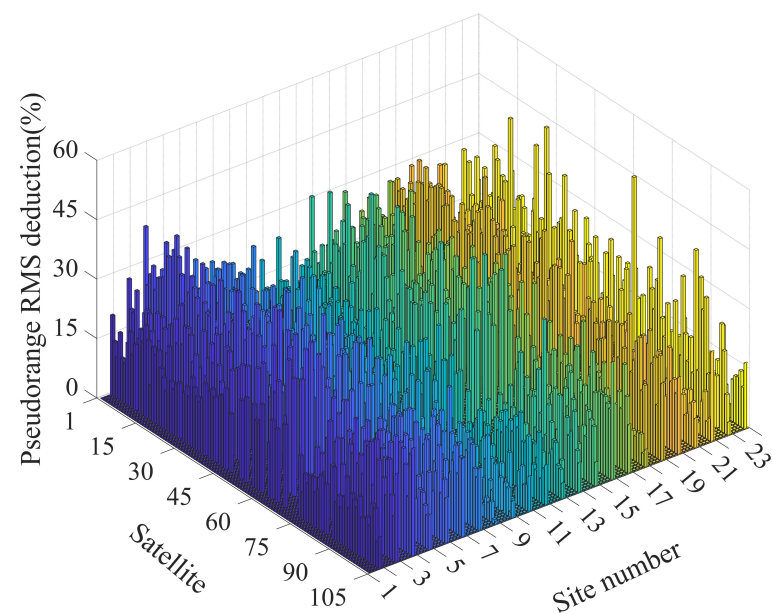


**Figure 4.** RMS reduction for pseudorange observation by  $MHM_{0.5}$  on DOY 267 in 2021.

**Table 3.** Averaged RMS reduction in the carrier-phase and pseudorange for the different systems using  $MHM_{0.5}$  and SF (Unit: %).

Scheme	Observation	GPS	Galileo	BDS
$MHM_{0.5}$	Carrier-phase	26.5	25.5	24.6
	Pseudorange	20.0	19.5	20.7
SF	Carrier-phase	25.0	23.6	24.6
	Pseudorange	18.4	16.8	19.6

PPP is also vulnerable to other unmodeled errors, such as the CME. Figure 5 shows the raw carrier-phase residuals of G13 for six stations which are distant from each other (as shown in Figure 1, red circle). The carrier-phase residuals show similar fluctuations at the six stations, ranging from 17.5 to 18.5 h. Due to the relatively long distances between stations, the presence of fluctuations cannot be solely attributed to the similar environments

at each station. Referring to the relevant inferences by Zheng et al. [2] in coordinate domains, the CME could have been mainly caused by satellite orbit and clock errors, as well as the components of unmodeled errors, which deteriorated the multipath modeling to some extent. Due to the larger measurement noise, the CME was not evident in the same period in the pseudorange residuals, as shown in Figure 6.

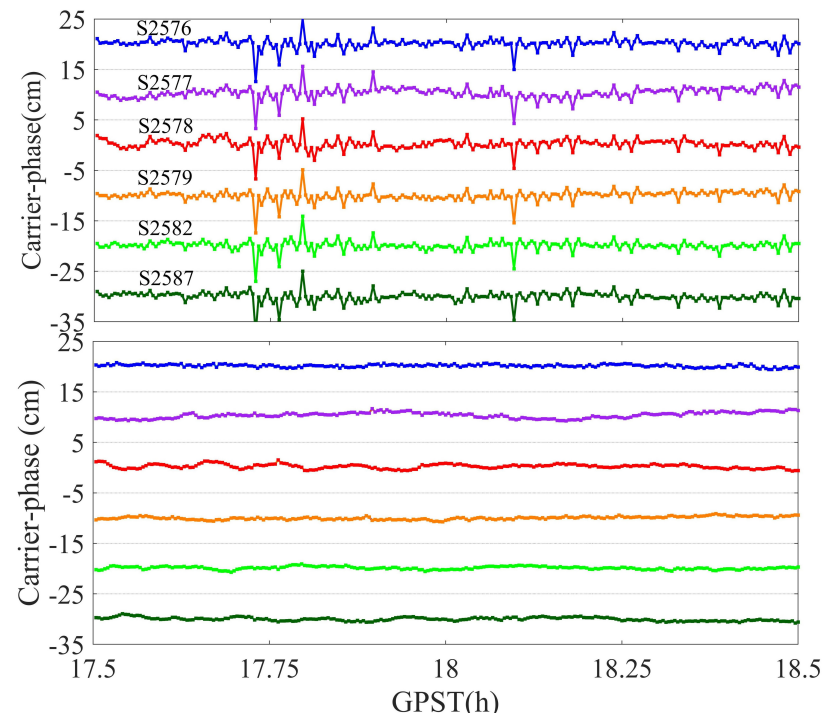


**Figure 5.** Carrier–phase residuals of the raw (**up**) and after CME was removed (**down**) G13 satellite for six stations on DOY 267 in 2021.

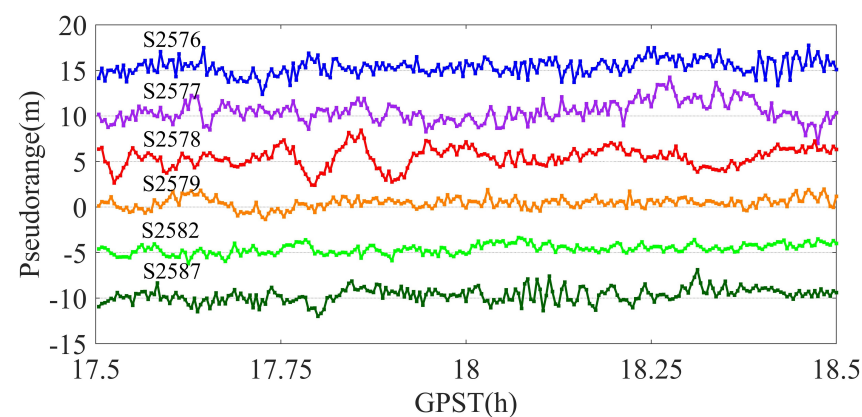


**Figure 6.** Raw pseudorange residuals of the G13 satellite for six stations on DOY 267 in 2021.

### 3.3. Performance of PPP-AR with Multipath Mitigation

The performance of multi-GNSS PPP-AR with multipath correction was evaluated. The time to first fix (TTFF) was used as an indicator of positioning performance, defined as the time required for the first ambiguity to be successfully resolved [41]. Table 4 presents a comparison of the average TTFF values for different schemes, including  $MHM_{0.5}$  and SF, across 23 stations. The results indicate that, in terms of TTFF improvement,  $MHM_{0.5}$  slightly outperformed SF. Compared with SF, the average  $MHM_{0.5}$  TTFF was decreased by about 0.3 min and 1.1 min for each scheme in the static and kinematic mode, respectively. In the kinematic mode, the TTFF of the GPS-only solution with  $MHM_{0.5}$  was reduced from 55.1 min to 51.2 min compared to the case without multipath correction. The GE solution

shortened by 21.5% to 16.9 min, while the GC solution was reduced by 37.5% from 25.3 min to 15.8 min. As expected, the GEC solution achieved the shortest TTFF of approximately 12.2 min. In static mode, after applying MHM<sub>0.5</sub>, the GPS-only PPP-AR achieved the first fixed solution within 20 min, and that of the dual system was approximately 12 min. The TTFF of the GEC solution was reduced to approximately 10 min.

The integrated system demonstrated superior positioning performance in comparison to the individual systems, indicating a substantial enhancement in both kinematic and static scenarios. The results substantiate that the addition of additional constellations effectively reduced the time to first fix (TTFF) for PPP-AR. On this basis, incorporating multipath correction further enhanced the TTFF performance of PPP-AR.

**Table 4.** Averaged TTFF of kinematic(K)/static(S) PPP-AR with different schemes (Unit: min).

Scheme	G		GE		GC		GEC	
	K	S	K	S	K	S	K	S
Uncor	55.1	27.1	20.5	13.6	25.3	14.9	16.0	10.5
MHM <sub>0.5</sub>	51.2	19.0	16.9	11.0	15.8	11.9	12.2	9.7
SF	52.8	19.2	18.4	11.5	16.3	12.2	13.1	10.0

In kinematic PPP-AR, the convergence time is defined as the minimum duration required to attain a horizontal accuracy of 10 cm and to sustain it for 10 consecutive epochs. In static PPP-AR, the horizontal accuracy requirement is enhanced to 5 cm and maintained within 5 cm for 10 consecutive epochs. The impact of multipath mitigation on the convergence time in real-time PPP-AR for G/GE/GC/GEC combinations was evaluated, and the statistical results of the averaged convergence time before and after multipath correction are shown in Table 5.

After employing MHM<sub>0.5</sub> for multipath correction in kinematic mode, the average convergence time for the GPS-only results was shortened by 56.4% to 18.2 min and shortened by 38.4% to 11.7 min for GE. It is worth noting that the GC was markedly shortened from 20.7 to 8.6 min, which is a more noticeable improvement compared to the GE solution. In the given scenario, the correction performance of the SF and MHM<sub>0.5</sub> was comparable. However, the SF model exhibited slightly better correction results for GPS compared to MHM<sub>0.5</sub>. The GEC solution achieved a significant reduction of 60.6% and converged in approximately 7 min in both correction models. In static mode, the GEC solution average convergence time was shortened by 33.6% from 12.5 to 8.3 min with MHM<sub>0.5</sub> correction, while the impact of SF was measured as 21.6%. From Table 5, it can be seen that multipath correction exhibited a clear enhancement in the convergence time of the different satellite combinations. This finding further suggests that, by correcting for multipath errors, rapid centimeter-level positioning is expected, even in scenarios with a suboptimal satellite distribution.

**Table 5.** Average convergence time for different system combinations using MHM<sub>0.5</sub> and SF in kinematic/static mode (Unit: min).

Mode	Scheme	G	GE	GC	GEC
Kinematic	Uncor	41.6	19.0	20.7	18.0
	MHM <sub>0.5</sub>	18.2	11.7	8.6	7.1
	SF	15.8	12.9	8.6	7.2
Static	Uncor	19.2	12.4	19.0	12.5
	MHM <sub>0.5</sub>	11.7	10.0	11.3	8.3
	SF	13.0	11.4	9.7	9.8

In order to compare and illustrate the convergence time of kinematic PPP-AR before and after multipath correction, we provide the percentage of stations converging within each time period within a 50-minute interval, as shown in Figure 7. In each subgraph, the orange bar chart represents the original results, while the green bar charts represent the results with multipath correction. In some instances, few observed GPS satellites may have caused the GPS PPP-AR to achieve convergence in more than 40 min [41]. Before applying multipath correction, the convergence time for most stations in GPS-only PPP-AR ranged from 15 to 45 min, with only 17.4% of stations converging within 20 min. In contrast, the convergence time for the GE solution was mostly within 25 min, while the GC solution showed a concentration of converged stations within the 15–35 min range. Including additional systems strengthened the satellite spatial geometry, leading to a noticeable reduction in PPP-AR convergence time. After applying multipath correction, approximately 47.8% of the stations achieved convergence within 20 min for GPS-only PPP-AR. Furthermore, the convergence performance of the GC solution showed substantial improvement, with most stations converging within 20 min, outperforming the GE results. Notably, the convergence time of the GC solution was significantly reduced after multipath correction. These findings are consistent with the residual processing results discussed in Section 3. The results indicated that multipath correction has a conspicuous impact on the convergence time for PPP-AR, particularly for the GEC combination solution, with approximately 80% of stations achieving convergence within 10 min after applying  $MHM_{0.5}$ .

Similarly, the convergence results of static PPP-AR are illustrated in Figure 8. A comparison between Figures 7 and 8 demonstrates that, across all schemes, the static convergence time was significantly shorter compared to the kinematic case. It is noteworthy that the impact of multipath correction on the static results was more consistent and stable across all stations. For instance, before applying multipath correction, the convergence time for the GPS-only PPP-AR of all stations varied from 10 to 40 min. However, after implementing the correction, convergence was achieved within 30 min, with approximately 78.3% of stations achieving convergence within 15 min (although some stations still required 20 to 30 min for convergence). Similarly, for the GE scheme, the convergence time ranged from 10 to 30 min before multipath correction, but after correction, the convergence time was primarily concentrated within 10 min. For GC and GEC, with the application of enhanced multipath error correction, 4.35% and 8.7% of the stations achieved convergence of PPP-AR within 5 min, respectively.

The positioning accuracy was defined as the RMS of the positioning error from the 300th epoch (75 min) to the last epoch after the start of positioning. To evaluate the improvement in multipath correction on the PPP-AR, the positioning accuracies of the four schemes were calculated after convergence. Figure 9 shows the kinematic PPP-AR positioning errors at station 2588 on DOY 267, 2021. There are fluctuations in the GPS-only positioning error series, and the maximum values of the east, north and up components reached 0.76, 0.27, and  $-0.33$  cm, respectively. With multipath correction, the GPS PPP-AR 3D positioning accuracies improved from 1.2, 1.2, and 2.6 cm to 1.1, 0.8, and 2.5 cm, and the convergence time decreased from 46.3 to 29.3 min. It is worth noting that the corrected GEC results achieved accuracies of 0.7, 0.8, and 1.5 cm within 2.3 min, significantly outperforming the other cases. Table 6 presents the statistics of the average PPP-AR positioning accuracies of the 23 stations. For GPS-only solutions, they were 1.42, 1.30, and 2.97 cm for the east, north, and up components. After multipath correction, the 3D accuracies were further improved by 18.3%, 15.4%, and 14.1%, to 1.16, 1.10, and 2.55 cm, respectively. Multipath correction had the most pronounced improvement for GEC, whose average positioning accuracy was improved by 30.2%, 4%, and 16.2% compared to GPS-only, GE, and GC, respectively.

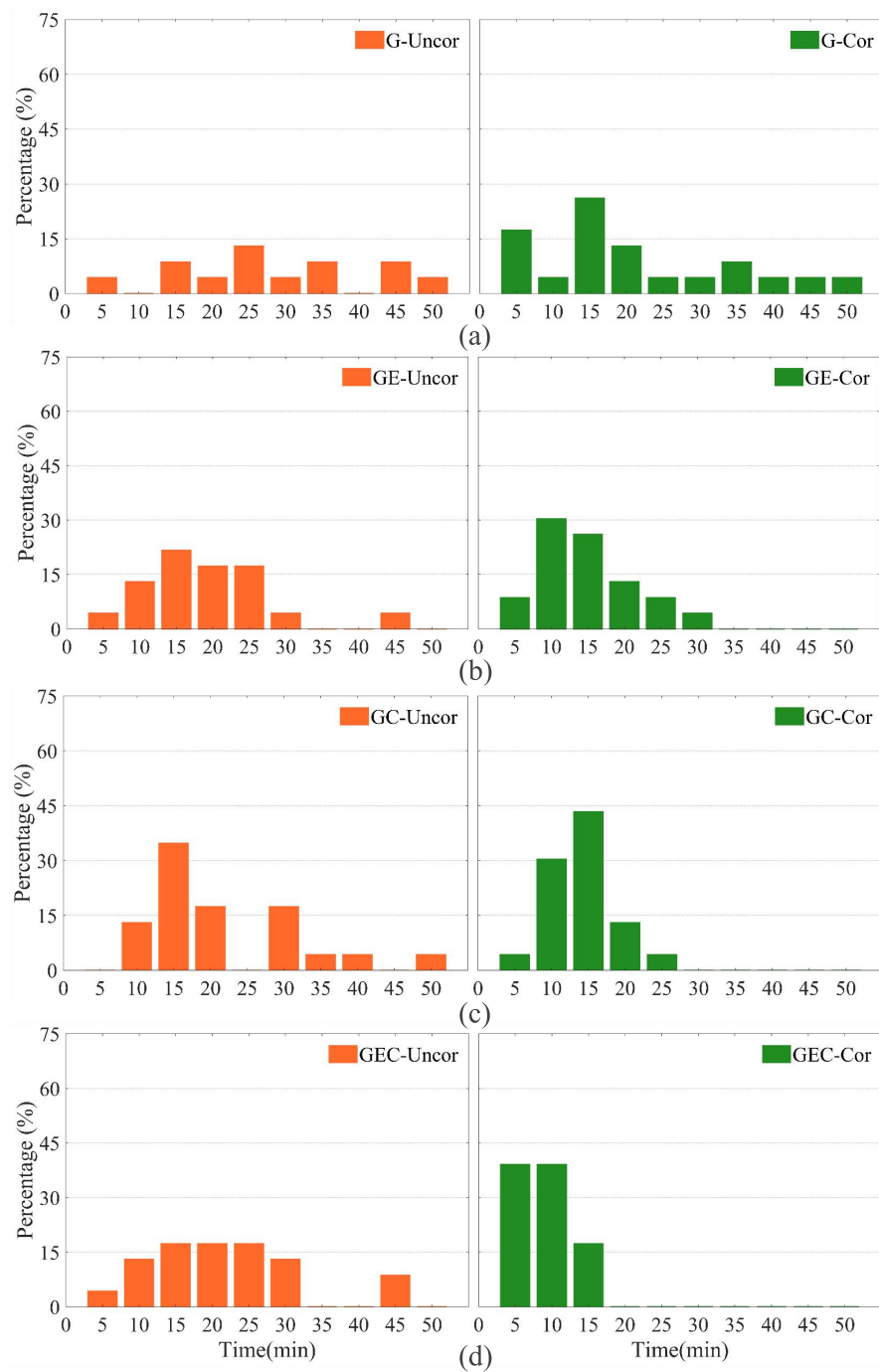


**Figure 7.** Kinematic PPP-AR convergence station statistics before (left) and after (right) multipath correction. (a) for GPS-only, (b) for GE, (c) for GC, and (d) for GEC solutions.

**Table 6.** The averaged positioning for Kinematic PPP-AR accuracy for all stations in the different schemes. (Unit: cm).

	G		GE		GC		GEC	
	Uncor	Cor	Uncor	Cor	Uncor	Cor	Uncor	Cor
East	1.42	1.16	1.11	1.07	1.40	0.93	0.97	0.94
North	1.30	1.10	0.85	0.72	1.35	0.98	0.88	0.70
Up	2.97	2.55	2.10	1.71	2.61	2.10	2.07	1.72

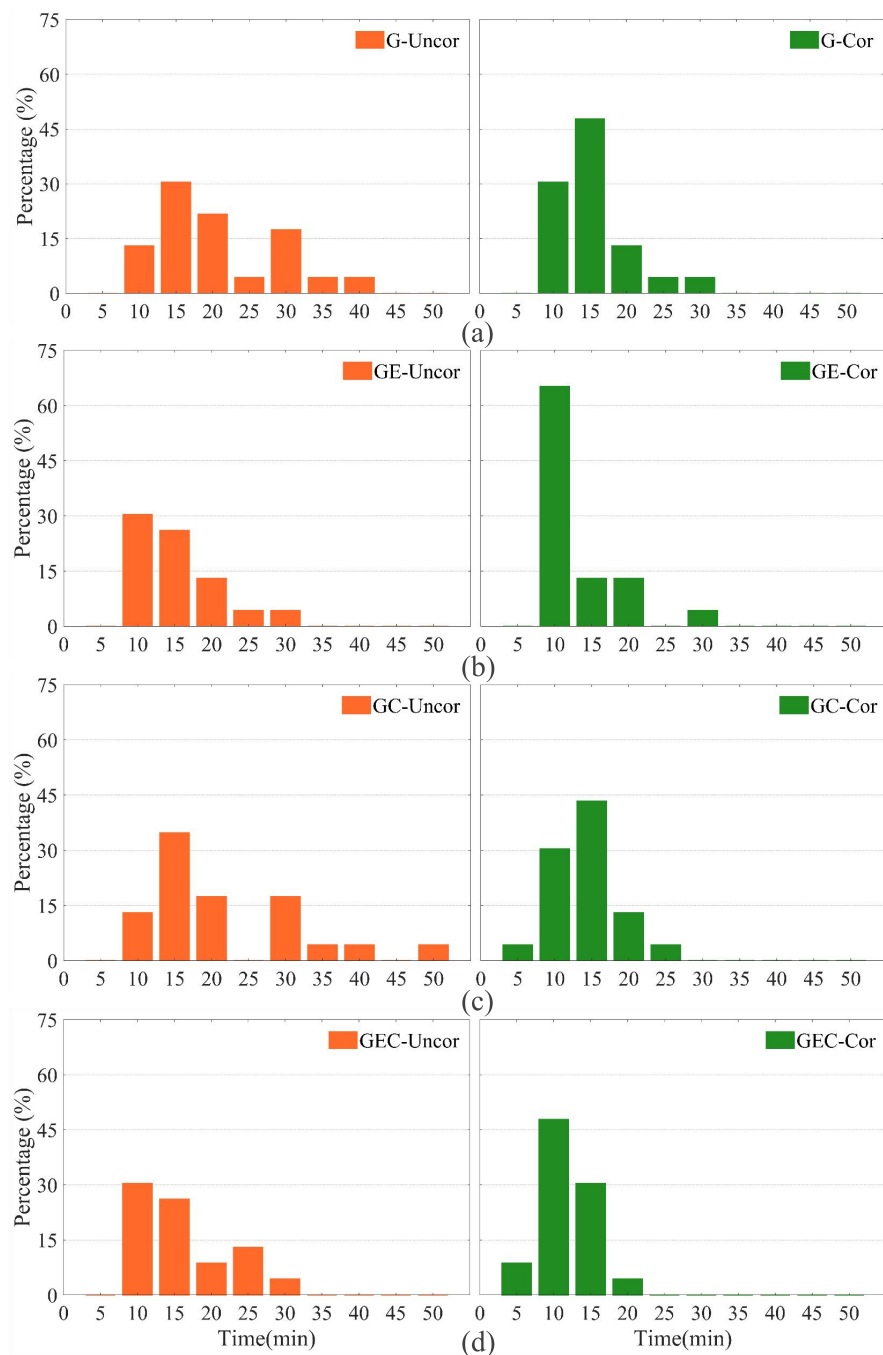


**Figure 8.** Static PPP-AR convergence station statistics before (left) and after (right) multipath correction. (a) for GPS-only, (b) for GE, (c) for GC, and (d) for GEC solutions.

The effectiveness of multipath correction in the static PPP-AR positioning mode was assessed. Figure 10 displays the 3D positioning errors of the static PPP-AR at station 2588 on DOY 267, 2021. Table 7 presents the positioning accuracy statistics for all 23 stations. Compared with kinematic PPP-AR, static PPP-AR required less time to achieve convergence and had better positioning accuracy. As shown, for GEC PPP-AR, the positioning accuracy improved significantly after multipath correction, which was ameliorated by 10.7%, 6.3%, and 45.4% to 0.50, 0.30, and 0.71 cm, respectively. Multipath correction significantly enhanced the positioning accuracy of the schemes, particularly in the vertical component. This improvement can be attributed to the fact that ambiguity resolution mainly contributed to the horizontal direction, where a high level of accuracy had already been achieved [3].

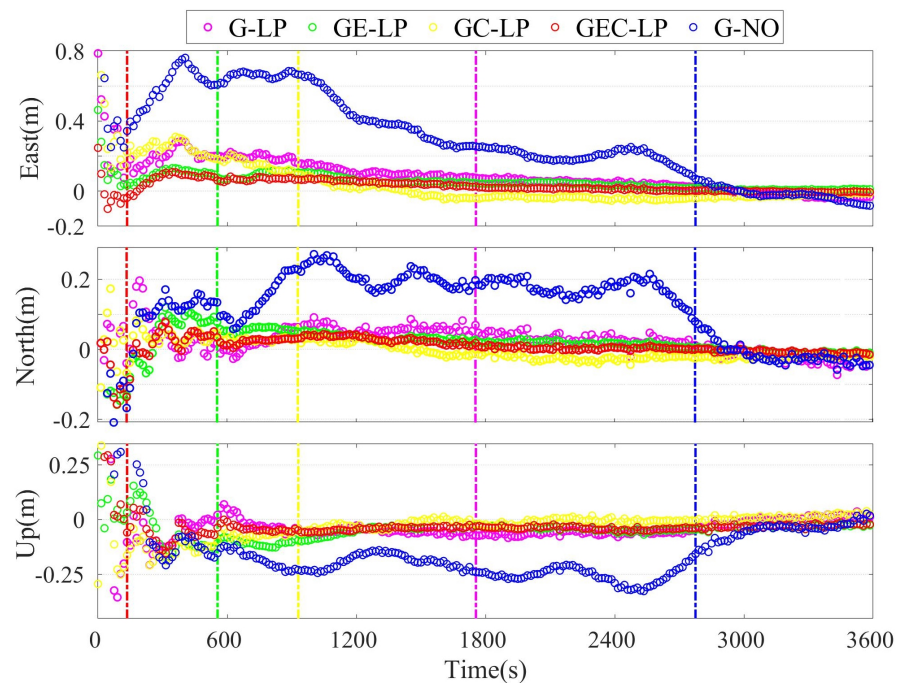


**Figure 9.** Kinematic PPP-AR positioning errors at station 2588 on DOY 267, 2021. G-NO denotes the GPS-only PPP-AR without multipath correction, while G-LP, GE-LP, GC-LP, and GEC-LP represent each PPP-AR solution with  $MHM_{0.5}$  correction. The vertical lines indicate the convergence time for each scheme.

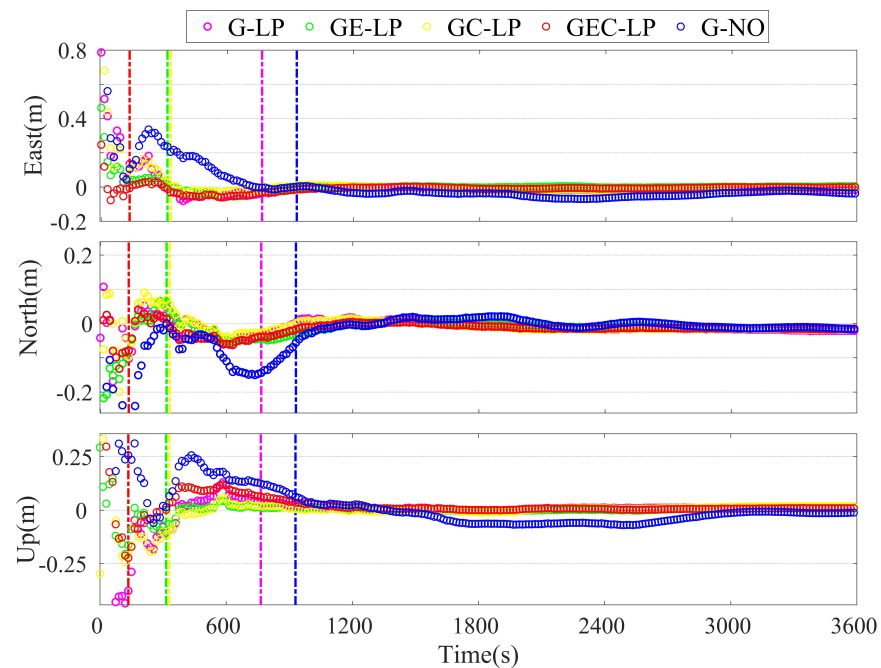


**Figure 10.** Static PPP-AR Positioning errors at station 2588 on DOY 267, 2021. G-NO denotes the GPS-only PPP-AR without multipath correction, while G-LP, GE-LP, GC-LP, and GEC-LP represent each solution with  $MHM_{0.5}$  correction. The vertical lines denote the convergence time for each scheme.

**Table 7.** The averaged positioning accuracy of static PPP-AR for all stations in the different schemes. (Unit: cm).

	G		GE		GC		GEC	
	Uncor	Cor	Uncor	Cor	Uncor	Cor	Uncor	Cor
East	0.51	0.47	0.53	0.45	0.52	0.47	0.56	0.50
North	0.33	0.32	0.34	0.32	0.33	0.32	0.32	0.30
Up	1.67	0.91	1.24	0.75	1.64	0.69	1.30	0.71

Table 8 lists the fixing rates of the different positioning combinations PPP-AR. The fixing rate is defined as the ratio of the fixed epoch number to the total number of epochs. It can be seen from the table that the improvement in fixing rates for kinematic and static PPP-AR due to multipath correction was minimal. However, a comparison of the different positioning combinations leads to the conclusion that a more favorable satellite geometric distribution had a more pronounced impact on enhancing the fixed rates.

**Table 8.** The average fixing rate of PPP-AR for all stations in the different schemes. (Unit: %).

Mode	Scheme	G	GE	GC	GEC
Kinematic	Uncor	96.2	98.5	98.0	99.3
	MHM <sub>0.5</sub>	96.6	98.6	99.4	99.7
	SF	96.6	98.6	99.0	99.7
Static	Uncor	97.6	99.5	99.2	99.8
	MHM <sub>0.5</sub>	98.0	99.8	99.8	100.0
	SF	98.0	99.7	99.6	99.9

We compared the positioning errors over consecutive days from DOY263 to DOY267 and calculated their Pearson correlation coefficients. Due to a higher accuracy in the east direction, the error correlation between different days was stronger compared to the other two directions. After the correction of multipath effects, the similarity in errors among the three directions decreased by approximately 0.3, to 0.5. These findings indicate that the periodic errors in the positioning accuracy were effectively reduced.

#### 4. Discussion

Comparing the positioning accuracy shown in Tables 6 and 7, it can be observed that the accuracy of the GPS corrected solution was comparable to the original solution of the combined system. This can be explained by fact that the introduction of new observations bolstered the satellite geometry but simultaneously introduced multipath errors [42]. Based on the experimental results in Figures 7 and 8, it can be observed that certain stations achieved rapid convergence after multipath correction. This finding further suggests that by correcting for multipath errors, rapid centimeter-level positioning is expected, even in scenarios with a suboptimal satellite distribution.

The performance of the SF method in the observation domain largely relies on the orbital repetition period of different GNSS satellites. The MHM model, in particular, benefits from a high-resolution grid to effectively correct errors. These methodologies capitalize on the spatio-temporal repetition characteristics of multipath errors and aim to mitigate their impact by leveraging statistical properties. However, one drawback is the need for long-term historical data to estimate the statistical model parameters. In practical scenarios, multipath signal parameters display dynamic variations, and the measurement noise properties change over time and across environments. This leads to an increase in the non-periodic trend component observed in phase and pseudorange residuals. Currently, the evaluation of multipath correction focuses on its impact on multi-system PPP-AR, requiring further investigation of its effects on multi-frequency approaches. To address these challenges, more efficient and adaptive algorithms are necessary, to establish a correlation model between multipath errors

and factors such as satellite elevation and azimuth. This would facilitate real-time prediction and correction of PPP-AR multipath errors. Machine learning techniques can be employed as promising approaches in this context.

## 5. Conclusions

In this study, we established MHM and SF models using PPP carrier-phase and pseudorange residuals extracted from the IF combination. We processed a 31-day dataset from 23 SAPOS stations, and the effects of multipath correction on real-time multi-GNSS PPP-AR were evaluated in both kinematic and static positioning modes. We calculated RMS reductions of carrier-phase and pseudorange residuals for multi-GNSS PPP-AR with MHM<sub>0.5</sub>, which showed 25.5% and 20.1% reductions, respectively. Conversely, when the SF method was used, the RMS reductions were 24.4% and 18.3%. For kinematic PPP-AR, after implementing MHM<sub>0.5</sub> for multipath correction, the average TTFF of G/GE/GC/GEC kinematic PPP-AR was shortened by approximately 7.0%, 17.7%, 37.5%, and 23.8%, respectively, the average convergence time for G/GE/GC/GEC was shortened by 56.4%, 38.4%, 58.5%, and 60.6% to 18.2, 11.7, 8.6, and 7.1 min. These results were consistent with the RMS statistic results of multipath correction. This study concludes that about 40% of the stations reached convergence within 5 min, while 80% of the stations achieved convergence within 10 min. The superior positioning accuracy for GEC PPP-AR was 0.94, 0.70, and 1.72 cm for the east, north, and up components, respectively. Meanwhile, in the static positioning mode, the average TTFF of G/GE/GC/GEC TTFF was shortened to 19.2, 11.5, 12.2, 10.0 min, and the average convergence time was 13.0, 10.0, 11.3, and 8.3 min, respectively. The superior positioning accuracy for static GEC PPP-AR was 0.5, 0.3, and 0.71 cm with three components. Multipath correction modestly improved the fixing rates for kinematic and static PPP-AR.

**Author Contributions:** Data curation, K.Z. and L.T.; Funding acquisition, K.Z. and K.L.; Methodology, K.Z.; Supervision, K.L.; Writing—original draft, K.Z. and L.T.; Writing—review and editing, L.T., K.L., M.C. and X.Z. All authors have read and agreed to the published version of the manuscript.

**Funding:** This study received financial support from the National Natural Science Foundation of China (Grant No. 42104015), the Key Research and Development Program of Hubei Province (Grant No. 2022BID010), and the Natural Science Foundation of Hubei Province (Grant No. 2021CFA001).

**Acknowledgments:** The authors express their gratitude to the Satellite Positioning Service of the German National Survey (SAPOS) for the GNSS observations that were generously provided, [https://www.opengeodata.nrw.de/produkte/geobasis/rb/sapos/gpps\\_archiv/](https://www.opengeodata.nrw.de/produkte/geobasis/rb/sapos/gpps_archiv/) (accessed on 1 January 2023) as well as the help of GFZ in providing precise products <ftp://ftp.gfz Potsdam.de/GNSS/products/mgex> (accessed on 1 January 2023).

**Conflicts of Interest:** The authors declare no conflict of interest.

## References

1. Zumberge, J.F.; Heflin, M.B.; Jefferson, D.C.; Watkins, M.M.; Webb, F.H. Precise point positioning for the efficient and robust analysis of GPS data from large networks. *J. Geophys. Res. Solid Earth* **1997**, *102*, 5005–5017. [[CrossRef](#)]
2. Zheng, K.; Zhang, X.; Sang, J.; Zhao, Y.; Wen, G.; Guo, F. Common-mode error and multipath mitigation for subdaily crustal deformation monitoring with high-rate GPS observations. *GPS Solut.* **2021**, *25*, 1–15. [[CrossRef](#)]
3. Li, X.; Zheng, K.; Li, X.; Liu, G.; Ge, M.; Wickert, J.; Schuh, H. Real-time capturing of seismic waveforms using high-rate BDS, GPS and GLONASS observations: The 2017 MW 6.5 Jiuzhaigou earthquake in China. *GPS Solut.* **2018**, *23*, 1–12. [[CrossRef](#)]
4. Gendt, G.; Dick, G.; Reigber, C.; Tomassini, M.; Liu, Y.; Ramatschi, M. Near real time GPS water vapor monitoring for numerical weather prediction in Germany. *J. Meteorol. Soc. Jpn. Ser. II* **2004**, *82*, 361–370. [[CrossRef](#)]
5. Teunissen, P.J.G. The least-squares ambiguity decorrelation adjustment: A method for fast GPS integer ambiguity estimation. *J. Geod.* **1995**, *70*, 65–82. [[CrossRef](#)]
6. Geng, J.; Teferle, F.N.; Meng, X.; Dodson, A.H. Towards PPP-RTK: Ambiguity resolution in real-time precise point positioning. *Adv. Space Res.* **2011**, *47*, 1664–1673. [[CrossRef](#)]
7. Li, X.; Ge, M.; Zhang, H.; Wickert, J. A method for improving uncalibrated phase delay estimation and ambiguity-fixing in real-time precise point positioning. *J. Geod.* **2013**, *87*, 405–416. [[CrossRef](#)]

8. MGEX Constellations—International GNSS Service (igs.org). Available online: <https://igs.org/mgex/constellations> (accessed on 1 August 2023).
9. Li, P.; Zhang, X.; Ren, X.; Zuo, X.; Pan, Y. Generating GPS satellite fractional cycle bias for ambiguity-fixed precise point positioning. *GPS Solut.* **2016**, *20*, 771–782. [[CrossRef](#)]
10. Li, P.; Jiang, X.; Zhang, X.; Ge, M.; Schuh, H. GPS + Galileo + Beidou precise point positioning with triple-frequency ambiguity resolution. *GPS Solut.* **2020**, *24*, 1–13. [[CrossRef](#)]
11. Veitsel, V.A.; Zhdanov, A.V.; Zhodzishsky, M.I. The mitigation of multipath errors by strobe correlators in GPS/GLONASS receivers. *GPS Solut.* **1998**, *2*, 38–45. [[CrossRef](#)]
12. Groves, P.D.; Jiang, Z.; Skelton, B.; Cross, P.A.; Lau, L.; Adane, Y.; Kale, I. Novel multipath mitigation methods using a dual-polarization antenna. In Proceedings of the 23rd International Technical Meeting of The Satellite Division of the Institute of Navigation (ION GNSS 2010), Portland, OR, USA, 21–24 September 2010; pp. 140–151.
13. Bilich, A.; Larson, K.M. Correction published 29 March 2008: Mapping the GPS multipath environment using the signal-to-noise ratio (SNR). *Radio Sci.* **2007**, *42*, 1–16.
14. Su, M.; Zheng, J.; Yang, Y.; Wu, Q. A new multipath mitigation method based on adaptive thresholding wavelet denoising and double reference shift strategy. *GPS Solut.* **2018**, *22*, 1–12. [[CrossRef](#)]
15. Genrich, J.F.; Bock, Y. Rapid resolution of crustal motion at short ranges with the global positioning system. *J. Geophys. Res. Solid Earth* **1992**, *97*, 3261–3269. [[CrossRef](#)]
16. Choi, K.; Bilich, A.; Larson, K.M.; Axelrad, P. Modified sidereal filtering: Implications for high-rate GPS positioning. *Geophys. Res. Lett.* **2004**, *31*, 178–198. [[CrossRef](#)]
17. Ragheb, A.E.; Clarke, L.; Edwards, S. GPS sidereal filtering: Coordinate- and carrier-phase-level strategies. *J. Geod.* **2007**, *81*, 325–335. [[CrossRef](#)]
18. Wang, M.; Wang, J.; Dong, D.; Li, H.; Han, L.; Chen, W. Comparison of three methods for estimating GPS multipath repeat time. *Remote Sens.* **2018**, *10*, 6. [[CrossRef](#)]
19. Zhong, P.; Ding, X.; Yuan, L.; Xu, Y.L.; Kwok, K.; Chen, Y. Sidereal Filtering Based on Single Differences for Mitigating GPS Multipath Effects on Short Baselines. *J. Geod.* **2010**, *84*, 145–158. [[CrossRef](#)]
20. Atkins, C.; Ziebart, M. Effectiveness of Observation-Domain Sidereal Filtering for GPS Precise Point Positioning. *GPS Solut.* **2015**, *20*, 111–122. [[CrossRef](#)]
21. Cohen, C.E.; Parkinson, B.W. Mitigating multipath error in GPS based attitude determination. *Guid. Control* **1991**, *1991* 53–68.
22. Fuhrmann, T.; Luo, X.; Knöpfler, A.; Mayer, M. Generating statistically robust multipath stacking maps using congruent cells. *GPS Solut.* **2015**, *19*, 83–92. [[CrossRef](#)]
23. Dong, D.; Wang, M.; Chen, W.; Zeng, Z.; Song, L.-M.; Zhang, Q.; Cai, M.; Cheng, Y.; Jima Lv. Mitigation of multipath effect in GNSS short baseline positioning by the multipath hemispherical map. *J. Geod.* **2016**, *90*, 255–262. [[CrossRef](#)]
24. Wang, Z.; Chen, W.; Dong, D.; Wang, M.; Cai, M.; Yu, C.; Zheng, Z.; Liu, M. Multipath mitigation based on trend surface analysis applied to dual-antenna receiver with common clock. *GPS Solut.* **2019**, *23*, 1–15. [[CrossRef](#)]
25. Zheng, K.; Zhang, X.; Li, P.; Li, X.; Ge, M.; Guo, F.; Sang, J.; Schuh, H. Multipath extraction and mitigation for high-rate multi-GNSS precise point positioning. *J. Geod.* **2019**, *93*, 2037–2051. [[CrossRef](#)]
26. Zou, X.; Li, Z.; Wang, Y.; Deng, C.; Li, Y.; Tang, W.; Fu, R.; Cui, J.; Liu, J. Multipath Error Fusion Modeling Methods for Multi-GNSS. *Remote Sens.* **2021**, *13*, 2925. [[CrossRef](#)]
27. Zhang, Z.; Dong, Y.; Wen, Y.; Luo, Y. Modeling, refinement and evaluation of multipath mitigation based on the hemispherical map in BDS2/BDS3 relative precise positioning. *Measurement* **2023**, *213*, 25112722. [[CrossRef](#)]
28. Lu, R.; Chen, W.; Dong, D.; Wang, Z.; Zhang, C.; Peng, Y.; Yu, C. Multipath mitigation in GNSS precise point positioning based on trend-surface analysis and multipath hemispherical map. *GPS Solut.* **2021**, *25*, 119. [[CrossRef](#)]
29. Zheng, K.; Tan, L.; Liu, K.; Li, P.; Chen, M.; Zeng, X. Multipath mitigation for improving GPS narrow-lane uncalibrated phase delay estimation and speeding up PPP ambiguity resolution. *Measurement* **2023**, *206*, 112243. [[CrossRef](#)]
30. Kouba, J.; Héroux, P. Precise Point Positioning Using IGS Orbit and Clock Products. *GPS Solut.* **2001**, *5*, 12–28. [[CrossRef](#)]
31. Odijk, D. Ionosphere-free phase combinations for modernized GPS. *J. Surv. Eng.* **2003**, *129*, 165–173. [[CrossRef](#)]
32. Kouba, J. A Guide to Using International GNSS Service (IGS) Products. 2009. Available online: <http://acc.igs.org/UsingIGSProductsVer21.pdf> (accessed on 1 August 2023).
33. Seepersad, G.; Bisnath, S. Reduction of PPP convergence period through pseudorange multipath and noise mitigation. *GPS Solut.* **2015**, *19*, 369–379. [[CrossRef](#)]
34. Lau, L.; Cross, P. Development and testing of a new ray-tracing approach to GNSS carrier-phase multipath modelling. *J. Geod.* **2007**, *81*, 713–732. [[CrossRef](#)]
35. Agnew, D.C.; Larson, K.M. Finding the repeat times of the GPS constellation. *GPS Solut.* **2007**, *11*, 71–76. [[CrossRef](#)]
36. Cai, C.; Gao, Y.; Pan, L.; Zhu, J. Precise point positioning with quad-constellations: GPS, Beidou, GLONASS and Galileo. *Adv. Space Res.* **2015**, *56*, 133–143. [[CrossRef](#)]
37. Ge, M.; Gendt, G.; Rothacher, M.; Shi, C.; Liu, J. Resolution of GPS carrier-phase ambiguities in precise point positioning (PPP) with daily observations. *J. Geod.* **2008**, *82*, 389–399. [[CrossRef](#)]

38. Dong, D.; Fang, P.; Bock, Y.; Webb, F.; Prawirodirdjo, L.; Kedar, S.; Jamason, P. Spatiotemporal Filtering Using Principal Component Analysis and Karhunen-Loeve Expansion Approaches for Regional GPS Network Analysis. *J. Geophys. Res. Solid Earth* **2006**, *111*, B3. [[CrossRef](#)]
39. Li, P.; Zhang, X. Precise Point Positioning with Partial Ambiguity Fixing. *Sensors* **2015**, *15*, 13627–13643. [[CrossRef](#)]
40. Boehm, J.; Niell, A.; Tregoning, P.; Schuh, H. Global mapping function (GMF): A new empirical mapping function based on numerical weather model data. *Geophys. Res. Lett.* **2006**, *33*. [[CrossRef](#)]
41. Li, P.; Zhang, X. Integrating GPS and GLONASS to accelerate convergence and initialization times of precise point positioning. *GPS Solut.* **2014**, *18*, 461–471. [[CrossRef](#)]
42. Geng, J.; Jiang, P.; Liu, J. Integrating GPS with GLONASS for High-Rate Seismogeodesy. *Geophys. Res. Lett.* **2017**, *44*, 3139–3146. [[CrossRef](#)]

**Disclaimer/Publisher’s Note:** The statements, opinions and data contained in all publications are solely those of the individual author(s) and contributor(s) and not of MDPI and/or the editor(s). MDPI and/or the editor(s) disclaim responsibility for any injury to people or property resulting from any ideas, methods, instructions or products referred to in the content.